A–D–A-Type Oligothiophenes for Small Molecule Organic Solar Cells: Extending the π-System by Introduction of Ring-Locked Double Bonds

*Roland Fitzner, Elena Mena-Osteritz, Karsten Walzer, Martin Pfeiffer, and Peter Bäuerle**

A series of novel acceptor–donor–acceptor oligothiophenes terminally substituted with the 1-(1,1-dicyanomethylene)-cyclohex-2-ene (DCC) acceptor has been synthesized. Structural, thermal, optoelectronic, and photovoltaic properties of the π-extended DCC*n*Ts (*n* = 1–4) are characterized and contrasted to the trends found for the series of parent dicyanovinyl (DCV)-substituted oligothiophenes DCV*n*T. The optoelectronic properties reveal the influence of the additional exocyclic, sterically fixed double bonds in *trans*-configuration in the novel DCC*n*T derivatives. A close correspondence for derivatives with equal number of double bonds, that is, DCC*n*Ts and DCV(*n* + 1)Ts, is identified. Despite having the same energy gap, the energy levels of the frontier orbitals, HOMO and LUMO, for the DCC-derivatives are raised and more destabilized due to the aromatization energy of a thiophene ring versus two exocyclic double bonds indicating improved donor and reduced acceptor strength. DCC-terthiophenes give good photovoltaic performance as donor materials in vacuum-processed solar cells (power conversion efficiencies ≤ 4.4%) clearly outperforming all comparable DCV4T derivatives.

1. Introduction

Over the recent years, research in organic solar cells (OSC) has attracted great attention fueled by the potential for a future large-scale production of clean and inexpensive organic photovoltaic devices onto flexible substrates using continuous roll-to-roll processes. In OSCs, the interface between p- and n-type semiconducting organic materials is used to separate the strongly bound electron–hole pairs, formed upon photoexcitation, into free charge carriers. Besides the use of π-conjugated polymers as photoactive components, π-conjugated oligomers, often denoted as "small molecules," are gaining increasing popularity as they offer small batch-to-batch variations providing high reproducibility.[1–5] In addition to standard solution-processing, molecularly defined materials allow for solvent-free processing by vacuum evaporation techniques.

Systematic structural optimization of the oligomer donor materials allowed for an increase in power conversion efficiencies (PCE) to impressive values of close to 10% for single junction small molecule organic solar cells (SMOSC). Chen and co-workers investigated soluble oligothiophene-based acceptor–donor–acceptor (A–D–A)-type donor materials comprising central benzodithiophene units and could improve PCE to outstanding 9.95%.[1,6] The groups of Bazan and Heeger developed highly efficient D^1–A–D^2–A–D^1-type co-oligomers bearing a central dithienosilole unit leading to PCEs of up to 9% in solution-processed bulk heterojunction (BHJ) solar cells.[2,7] Very recently, Holmes and co-workers reported an efficiency of 7.9% for a vacuum-processed BHJ device using a triarylamine-benzothiadiazole-based D–A donor material,[8] which was introduced before by Wong and co-workers reaching PCEs of 6.8%.[9] Very recently, Cnops et al. published a vacuum-processed three layer device in a cascade architecture combining sexithiophene as donor and two subphthalocyanines as acceptors reaching a remarkable PCE of 8.4%.[10]

Our group explored the family of acceptor–donor–acceptor (A–D–A)-type oligothiophenes representing an efficient and well-investigated family of donor materials for vacuum-processed SMOSC. In particular, 2,2′-dicyanovinyl (DCV) as acceptor proofed to be ideal in order to achieve the optimal optoelectronic properties in the series of DCV*n*Ts (**Scheme 1**). In the first very promising solar cell application, butyl-substituted quinquethiophene DCV5T-Bu was deployed in SMOSC devices yielding a PCE of 3.4%.[11] Meanwhile, this material class has been extensively explored by the synthesis and characterization of several series of DCV*n*T oligomers. For example, by variation of the oligothiophene chain length, important structure–property relationships have been derived correlating the number of thiophene units in the conjugated backbone[12] or the length of the alkyl side chains with optoelectronic properties and photovoltaic performance.[13] A correlation between the packing of molecules in the solid state obtained from X-ray data and photovoltaic performance was established in a series

R. Fitzner, Dr. E. Mena-Osteritz, Prof. P. Bäuerle
Institute of Organic Chemistry II and Advanced Materials
University of Ulm
Albert-Einstein-Allee 11, 89081 Ulm Germany
E-mail: peter.baeuerle@uni-ulm.de
Dr. K. Walzer, Dr. M. Pfeiffer
Heliatek GmbH
Treidlerstrasse 3, 01139 Dresden, Germany
R. Fitzner
Heliatek,GmbH, Sedanstraße 14, 89077 Ulm, Germany

DOI: 10.1002/adfm.201404210

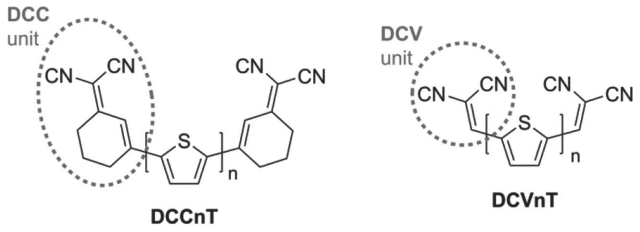

Scheme 1. Molecular structures of DCC- and DCV-capped oligothiophene series DCC*n*T and DCV*n*T.

of DCV-capped quaterthiophenes with systematic variation of the alkyl substituents identifying methyl-substituted DCV4T-Me as best-performing tetramer (PCE = 3.8%).[14] The optimization of the positioning of methyl substituents along the conjugated oligothiophene backbone in a series of quinquethiophenes led to excellent PCE values of 8.3% in single junction and 9.7% in multi junction cells, measured for the centrally methylated derivative.[15]

As the next step on the road to optimized A–D–A-type oligothiophene donor materials, we aspired to enlarge the conjugated π-system by introducing additional double bonds between the oligothiophene core and the electron-withdrawing DCV units. We endeavored to avoid structural *cis*/*trans* isomerism and to ensure thermal stability by integrating them into a cyclohexene ring.[16] In this contribution, we report on a novel series of A–D–A-type oligothiophenes bearing 1-(1,1-dicyanomethylene)-cyclohex-2-ene (DCC) units at both α-termini (DCC*n*T). Structural, thermal, optoelectronic, and photovoltaic properties were characterized and contrasted to the trends found for the series of dicyanovinyl-substituted oligothiophenes DCV*n*T, reported earlier (Scheme 1).

2. Results and Discussion

2.1. Synthesis

For the synthesis of the shorter DCC*n*T derivatives, bromocyclohexenone 3 was reacted with *bis*stannylated thiophene 1 or bithiopene 2 in Pd-catalyzed Stille-type cross-coupling reactions to afford diketo derivatives 4 and 5. Subsequent Knoevenagel condensation with malonitrile using β-alanine as the catalyst afforded target oligomers DCC1T and DCC2T in good yields (**Scheme 2**).

The longer less soluble DCC3T and DCC4T oligomers were synthesized by Stille-type cross-coupling reactions of DCC-substituted bromothiophene 9 with stannyl derivatives 1, 2, or 3,4-dimethylthiophene 10 as central building blocks yielding oligomers DCC3T, DCC4T, or DCC3T-Me, respectively. In order to obtain building block 9, 2,5-dibromothiophene was monolithiated with *n*-butyl lithium and quenched with methoxycyclohexenone 7 to yield ketone 8. Knoevenagel condensation with malonitrile provided DCC-substituted bromothiophene 9 as terminal building block.

2.2. Thermal Properties and Solubility

Differential scanning calorimetry (DSC) was used to investigate the thermal properties of all DCC*n*Ts. The decomposition onset temperatures (T_d) estimated from the onset of the exothermic signals in the DSC traces (**Figure 1**) are compiled in **Table 1**. Thermal degradation of the DCC*n*Ts occurred between 344 °C for DCC1T and 375 °C for DCC3T-Me. This indicates a high, but somewhat reduced thermal stability in comparison to the alkyl free DCV*n*Ts, which exhibited decomposition onset temperatures of about 400 °C.[12c] The DCC*n*T derivatives up to the trimers sublimed at temperatures between 250 and 280 °C ($p \approx 10^{-6}$ mbar) yielding crystalline material of high purity in almost quantitative yield. The sublimation of DCC4T occurred at significantly higher temperatures around the melting point and led to poor yields due to material decomposition.

Melting temperatures (T_m) of the DCC*n*Ts (Table 1) were determined from the onset of the endothermic signals in the DSC traces. All DCC*n*T derivatives exhibited high melting points between 290 and 333 °C which is an important requirement for efficient sublimation of the materials from the solid phase. In order to compare and to illustrate trends in the melting behavior of both oligothiophene series, in **Figure 2** the melting temperatures of the DCC*n*Ts and DCV*n*Ts are plotted versus the number of thiophene rings in the respective oligomer.

Comparing oligomers with identical oligothiophene cores, the DCC-substituted derivatives melted at higher temperatures than their DCV-capped analogues. This indicates that the two additional cyclohexene rings in the molecular structure of the DCC*n*Ts, which increase the molecular weight by 132 g mol^{-1} compared to the DCV*n*Ts, induce additional intermolecular interactions. The differences in melting points between DCC*n*Ts and DCV*n*Ts (ΔT_m in Table 1) diminished with increasing oligomer length from ΔT_m = 47 °C for the 1T to 13 °C for the 4T derivatives. As the number of thiophene units increases, the oligothiophene core dominates the molecular structure and the intermolecular forces. As we have shown previously for the DCV*n*T series, the DCC*n*T oligomers as well exhibited an odd–even effect of the melting points with respect to the number of thiophene units. Even-numbered DCV*n*Ts and DCC*n*Ts melt at significantly higher temperatures compared to their odd-numbered homologues. This trend may originate from a variance in molecular dipoles caused by differences in molecular symmetry between odd- and even-numbered oligomers.[10] The methylated oligomers DCC3T-Me, DCV3T-Me, and DCV5T-Me exhibited higher melting temperatures in comparison to the corresponding alkyl free derivatives which indicates additional intermolecular interactions induced by the methyl groups. Compared to their nonalkylated analogues, DCC3T-Me and DCV5T-Me exhibited similar increases in melting temperature (ΔT_m = 15 °C and 14 °C, respectively), while DCV3T-Me showed a larger enhancement in melting point (ΔT_m = 38 °C).

Maximum solubilities of DCC*n*Ts and DCV*n*Ts in dichloromethane were determined up to the tetramers. The corresponding values are compiled in Table 1 and plotted versus the number of thiophene units in the oligothiophene backbone (Figure 2). Despite having higher melting points, the DCC*n*Ts displayed enhanced solubility in this solvent compared to their DCV-substituted counterparts. Compared to the DCV group, this might be a result of enhanced flexibility and greater rotational freedom of the DCC acceptor

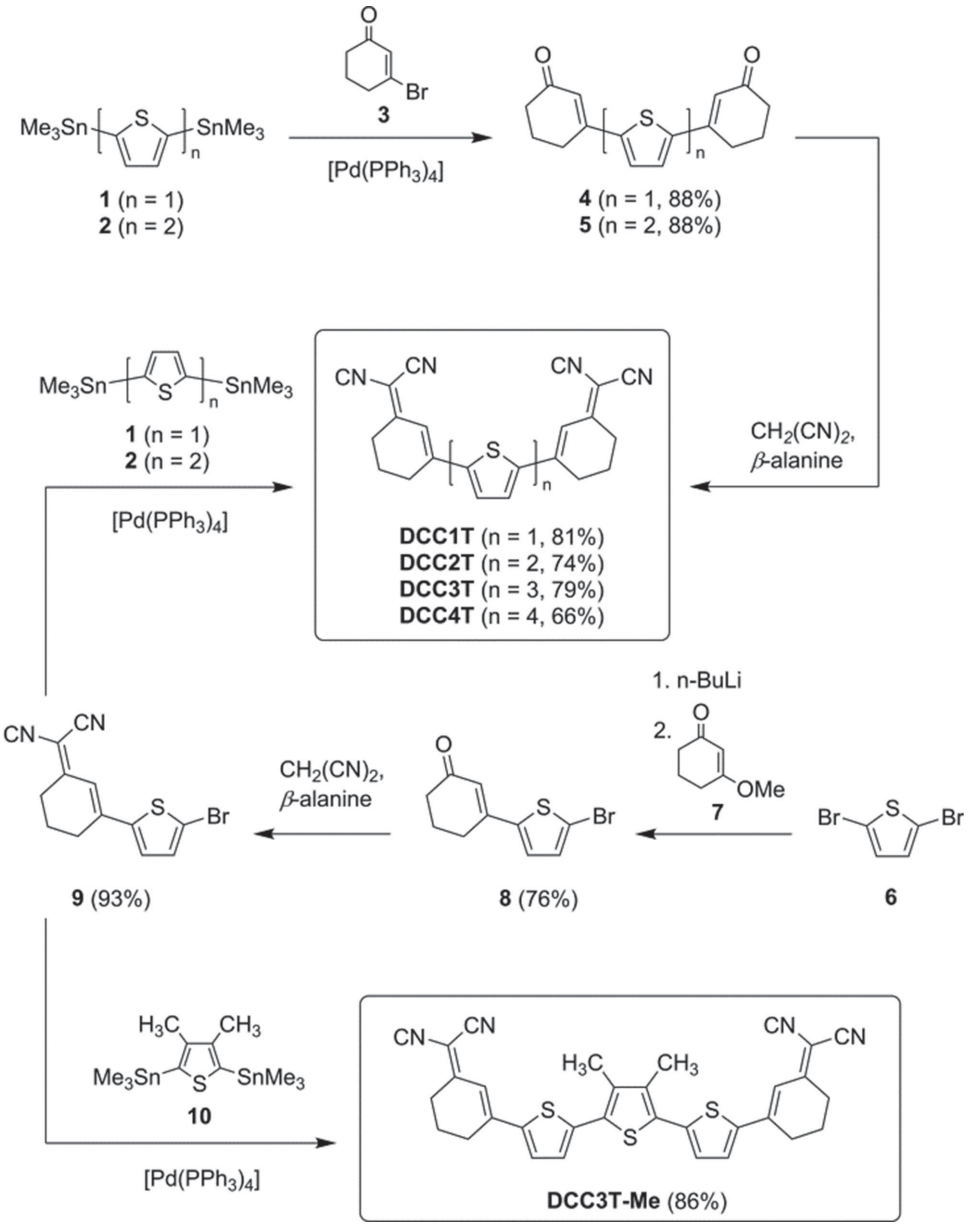

Scheme 2. Synthesis of DCC*n*T oligomers.

moiety around the bond to the oligothiophene core. In both oligomer series, maximum solubilities showed an odd–even effect with respect to the number of thiophene units, where oligomers with an even number of thiophenes are less soluble than those containing an odd number. This trend is the reverse of that found for the melting point temperatures. Methylated derivatives DCC3T-Me and DCV3T-Me were less soluble in dichloromethane compared to the corresponding alkyl free derivatives which is in accordance with the trend observed in melting points. Compared to the extremely insoluble alkyl free or methylated DCV*n*Ts, the solubilizing effect of the DCC acceptor moieties might be still not sufficient to enable a reliable fabrication of organic solar cells by solution-processing.

2.3. X-Ray Structure Analysis

Single crystals of DCC3T-Me were obtained by vacuum gradient sublimation. X-ray structure analysis provided valuable information about molecular geometry and packing and revealed notable similarities to the crystal structure of methylated DCV-capped quinquethiophene DCV5T-Me, which has the same substitution pattern, the same number of rings, and was reported earlier,[15a] including efficient π–π-stacking of the oligothiophene cores. The molecular structures of both oligomers will be compared, followed by an analysis of the crystal packing and intermolecular interactions. The crystals of DCC3T-Me and DCV5T-Me belong to the monoclinic space group C2/c with two molecules in the unit cell. The molecular structures

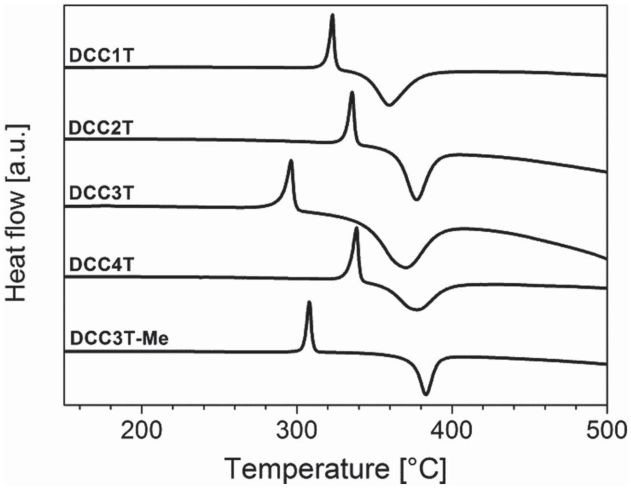

Figure 1. DSC traces of DCC*n*Ts measured under argon flow at a heating rate of 10 °C min^{-1}.

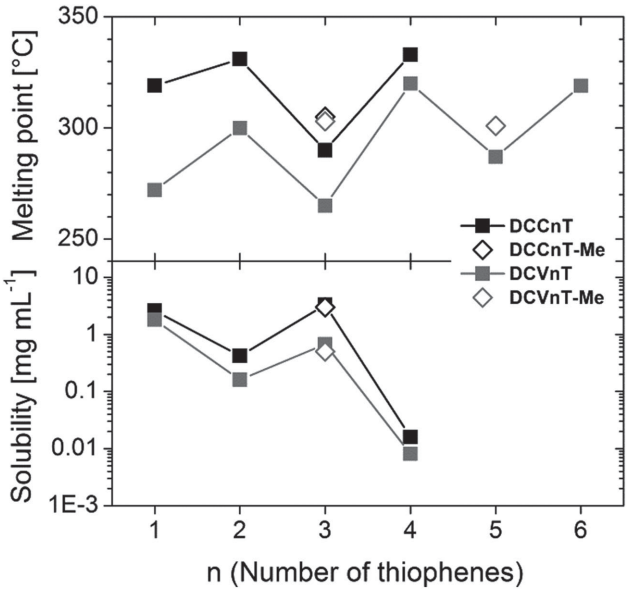

Figure 2. Melting points (top) and maximum solubilities in dichloromethane at room temperature (bottom) of DCC*n*Ts and DCV*n*Ts versus the number of thiophene units in the oligothiophene backbone.

of both oligomers display C_2 symmetry with the thiophene rings in an all-*anti*-conformation and the DCC or DCV units adopting *syn*-conformations with respect to the sulfur atoms of the terminal thiophene rings (**Figure 3**). The terminal double bonds of the acceptor units take very similar orientations with respect to the long molecular axis forming angles of 118° and 114° for DCC3T-Me and DCV5T-Me, respectively. Both oligomers displayed almost planar oligothiophene backbones, whereas the inter-ring dihedral angles are particularly small for DCC3T-Me (0.7°) compared to DCV5T-Me (5°, 7°). The DCC cyclohexene rings in the DCC3T-Me structure adopt half-chair conformation, in which the ring double bond is nearly coplanar with the adjacent thiophene ring (2.4°). In both structures, the dicyanomethylene moieties are significantly twisted out of the oligothiophene plane by 24° and 8° for DCC3T-Me and DCV5T-Me, respectively. This twist appears to be an effect of the particular molecular packing behavior observed for both oligomers, vide infra.

In **Figure 4** the crystal packing of DCC3T-Me is presented and compared to the very similar molecular arrangement observed for DCV5T-Me.[15] A common feature is the antiparallel alignment of the molecules on their long molecular axes, giving rise to the formation of ribbon-like structures (Figure 4a). This arrangement is favored by electrostatic CH...NC interactions between the terminal acceptor units of neighboring molecules (blue lines in Figure 4a and **Table 2**). In both crystal structures, adjacent molecular ribbons are offset from co-planarity by half the π–π-stacking distance (see side views in Figure 4b). The ribbons stabilize by CH···NC quasi hydrogen-bonding interactions between vinylic cyclohexenyl hydrogens and cyano nitrogen atoms (red lines in Figure 4a, top).

The DCV5T-Me crystal structure contains similar interactions between cyano nitrogen atoms and thienyl hydrogen atoms (red lines in Figure 4a, bottom).

Figure 4c depicts the molecular packing in the π–π-stacking direction. Both oligomers form slipped π–π-stack assemblies with slip angles of 41° or 57°, for DCC3T-Me and DCV5T-Me, respectively. The π–π-stacking molecular distances of 3.46 Å in DCC3T-Me are identical to the value obtained for DCV5T-Me (3.46 Å). Thus, the introduction of the DCC rings in the DCC3T-Me structure does not impair efficient π–π-interactions. Besides that, CH···π intermolecular interactions involving methyl- or cyclohexene hydrogens appear in both crystal structures (green and orange lines in Figure 4c). As a measure for the overall packing density, the Kitaigorodskii packing coefficients C_K were determined for both crystal structures by dividing the occupied molecular van der Waals volume by the total volume of the unit cell. Comparing DCC3T-Me and DCV5T-Me, the DCC-substituted oligomer exhibited a somewhat larger coefficient

Table 1. Thermal properties and maximum solubilities of DCC*n*Ts and DCV*n*Ts in dichloromethane.

Oligomer	T_m [°C]	T_d (DSC) [°C]	Solubility [mg mL^{-1}]	Oligomer	T_m [°C]	Solubility [mg mL^{-1}]	ΔT_m [°C]
DCC1T	319	343	2.6	DCV1T	272	1.8	47
DCC2T	331	362	0.42	DCV2T	300	0.16	31
DCC3T	290	340	3.3	DCV3T	265	0.67	25
DCC3T-Me	305	375	3.0	DCV3T-Me	303	0.50	2
DCC4T	333	352	1.6×10^{-2}	DCV4T	320	8.1×10^{-3}	13

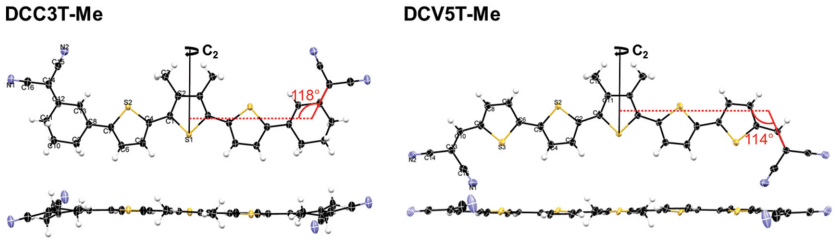

Figure 3. ORTEP diagrams (50% ellipsoids) of DCC3T-Me (left) and DCV5T-Me (right).

(0.709) than the DCV-capped derivative (0.674) indicating more efficient 3D packing. In consideration of identical π–π-stacking distances, this finding supports the closer molecular packing observed between the ribbons in the DCC3T-Me crystal structure (7.54 Å vs 7.95 Å for DCV5T-Me, Figure 4a).

Figure 5 highlights the alignment of adjacent DCC units in the DCC3T-Me crystal structure. Neighboring DCC groups form a linear zipper-like network, which is brought about by the two types of centrosymmetric interaction motifs (blue and red lines) described above. The well polarizable vinyl-hydrogens of the DCC moiety stabilize the arrangement by nonclassical hydrogen bond interactions.

2.4. Optoelectronic Properties

Optical absorption spectra of the DCC*n*T series determined in dichloromethane solution are presented in comparison to the DCV*n*T spectra in **Figure 6**. The corresponding values are compiled in **Table 3**. All DCC*n*Ts showed broad absorption profiles in the visible region. The absorption bands exhibited bathochromic shifts and increasing molar absorptivity with growing number of thiophene units indicating efficient conjugation throughout the π-system. The maximum absorption wavelengths λ_{max}^{abs} and the corresponding extinction coefficients ε_{max} of the DCC*n*Ts coincide well with the values determined for the DCV*n*T compounds comprising one additional thiophene unit, respectively. The bathochromic shift caused by the two additional cyclohexene double bonds in the DCC*n*Ts is therefore equivalent to adding one extra thiophene unit in the DCV*n*T series. DCV*n*T spectra showed increasing vibronic structure with decreasing number of thiophene units. DCC*n*T π–π^* absorption bands, in contrast, are structureless even for the shortest oligomer DCC1T. Compared to the DCV group, this may be attributed to a lower energy barrier of rotation of the DCC unit around the bond to the oligothiophene backbone. The DCV*n*Ts exhibit attractive intramolecular interactions between the sulfur atoms of the terminal thiophene rings and a DCV cyano group hindering rotation of the acceptor groups.[12c] Owing to the reduced conjugation of the oligothiophene core in solution, methylated DCC3T-Me displayed a slightly blue-shifted ($\Delta\lambda_{max}$ = 10 nm) and broadened absorption band with reduced molecular absorptivity compared to nonalkylated DCC3T. This is consistent with the behavior of alkyl substituted DCV*n*T derivatives.

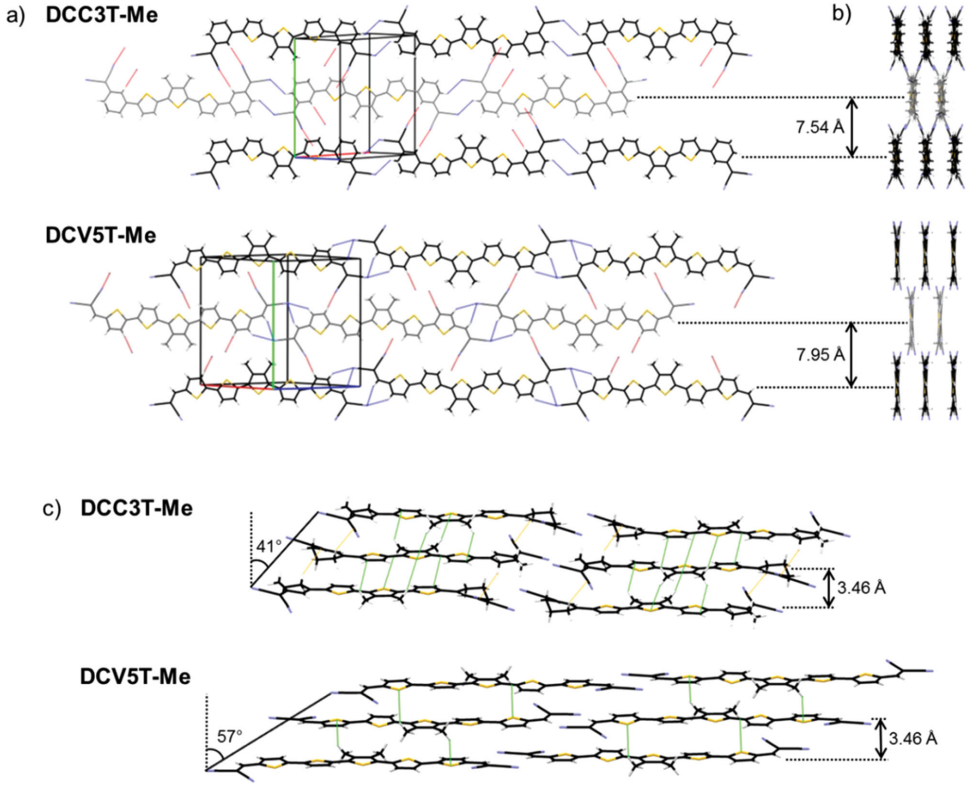

Figure 4. View of the crystal packing of DCC3T-Me and DCV5T-Me in a) the molecular plane, b) end view of the ribbone-like structures, and c) view perpendicular to the molecular plane showing the π–π-stacking of the molecules.

Table 2. Distances corresponding to intermolecular close CH···NC contacts in the crystal structures of DCC3T-Me and DCV5T-Me.

Oligomer	Close contacts (color code in Figure 8)	d [Å]	d–d_{vdW} [Å]
DCC3T-Me	N1···H11A (blue)	2.673	–0.077
	N2···H13 (red)	2.598	–0.152
DCV5T-Me	N2···H10 (blue)	2.553	–0.197
	N2···H8 (blue)	2.709	–0.041
	N1···H7 (red)	2.589	–0.161

Emission spectra of the DCC*n*Ts and DCV*n*Ts measured in dichloromethane solution are depicted in **Figure 7**. The emission maxima shifted bathochromically upon elongation of the π-system (Table 3). Unlike in the absorption spectra, the emission bands of the shorter DCC*n*Ts up to DCC3T showed vibronic structure which indicates a higher degree of structural rigidity and planarity of the molecules in the electronically excited state compared to the ground state. Compared to alkyl-free DCC3T, the emission band of methyl-substituted DCC3T-Me is less structured which may be due to increased rotational disorder in the oligothiophene backbone. Within the DCV*n*T series, a gradual increase in Stokes shift with increasing number of thiophene units from 320 cm^{-1} for DCV1T to 1803 cm^{-1} DCV6T was determined. However, all nonalkylated DCC*n*Ts displayed similar and significant Stokes shifts between 1282 cm^{-1} for DCC2T and 1547 cm^{-1} for DCC4T suggesting substantial differences in the electron distribution and molecular dipole moment between the ground state and excited state. Alkylated DCC3T-Me displayed the largest Stokes shift of 1883 cm^{-1} within the DCC*n*T series.

Figure 8 shows absorption and emission spectra of DCC3T and DCC3T-Me in thin films of equal thickness fabricated by vacuum-deposition. Compared to solution spectra, absorption and emission bands are red-shifted and significantly broadened in thin films for both oligomers indicating planarization and favorable ordering of the molecules in the bulk. Absorption profiles of the terthiophene derivatives are very similar with maximum optical densities of 0.46 and 0.45 at 544 and 547 nm for DCC3T and DCC3T-Me, respectively. Compared to DCC3T (λ_{max}^{em} = 736 nm), methylated DCC3T-Me showed a slightly increased Stokes shift in the thin film with an emission maximum of 766 nm. The optical gaps of the DCC*n*T

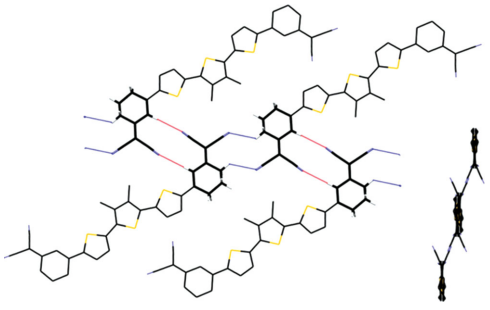

Figure 5. Intermolecular CN···HC close contacts between adjacent DCC groups in the crystal structure DCC3T-Me (side-view along the molecular axis in inset).

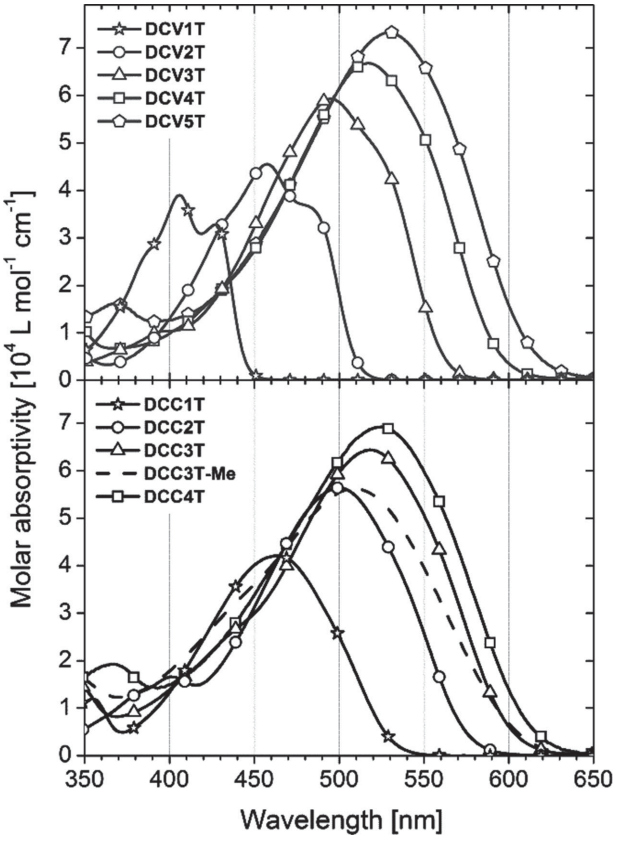

Figure 6. Absorption spectra of DCC*n*T (bottom) and DCV*n*T oligomers (top) measured in dichloromethane at room temperature.

series determined from the onset of absorption in solution spectra diminished from 2.33 eV for DCC1T to 2.03 eV for DCC4T. In thin films, the optical gaps of the terthiophene derivatives DCC3T and DCC3T-Me (E_g^{opt} = 1.79 eV) are reduced compared to the solution by 0.26 and 0.28 eV, respectively, which is comparable to the shifts determined for the DCV*n*T derivatives (ΔE_g = 0.33–0.35 eV).[12c] Cyclic voltammograms of the DCC*n*T oligomers were determined in 0.1 molar solutions of tetrabutyl ammonium hexafluorophosphate ($TBAPF_6$) in dichloromethane and are displayed in **Figure 9**a. The corresponding data are compiled in Table 3. DCC1T and DCC2T showed a single reversible oxidation wave within the accessible electrochemical window indicating the formation of stable radical cations. For the longer oligomers DCC3T, DCC3T-Me, and DCC4T two reversible one-electron oxidation processes were detected corresponding to the generation of stable radical cations and dications. The first oxidation potential is gradually shifted to lower values with the extension of the π-conjugated system from DCC1T (E_{Ox1} = 1.24 V) to DCC4T (E_{Ox1} = 0.63 V) concomitant with the increased delocalization of the radical cations. All nonalkylated DCC*n*Ts displayed reversible reduction signals, which are attributed to the generation of stable radical anions localized on each acceptor group. In comparison to the DCV*n*T oligomers, which exhibit only quasi-reversible reduction waves, the DCC acceptor moiety further stabilizes radical anionic species. In contrast to the effect seen in the oxidation, the reduction potentials are less

Table 3. Optoelectronic data of the DCC*n*T oligomers.

Oligomer	λ_{max}^{abs} [nm]	ε_{max} [L mol^{-1} cm^{-1}]	E_g^{opt} a) [eV]	λ_{max}^{em} [nm]	Stokes shift b) [cm^{-1}]	E_{Ox} [V]	E_{Red} [V]	E_{Homo} c) [eV]	E_{LUMO} c) [eV]	E_g^{CV} [eV]
DCC1T	463	42 100	2.33	587 (547)	1517	1.24	–1.21	–6.31	–3.94	2.37
DCC2T	500	56 400	2.15	595 (622)	1282	0.98	–1.29	–6.01	–3.84	2.17
DCC3T	519	64 400	2.07	624 (660)	1518	0.68, 1.08	–1.43	–5.71	–3.71	2.00
DCC3T-Me	509	56 200	2.05	651	1883	0.63, 1.05	–1.47	–5.69	–3.64	2.05
DCC4T	525	69 300	2.03	669	1547	0.63, 0.93	–1.46	–5.64	–3.68	1.96

a)Estimated using the onset of absorption in solution spectra; b)Calculated as difference between the 0–0 vibronic transitions of absorption and emission spectra, determined by mathematical Gaussian deconvolution; c)Calculated from onset values of the first oxidation and reduction waves setting the ferrocene HOMO energy to –5.1 eV versus vacuum.

affected by the enlargement of the π-system and E_{Red} decreased only from –1.21 V for DCC1T to –1.46 V for DCC4T because the negative charges are rather localized on the electron-withdrawing DCC acceptor moieties.

HOMO and LUMO frontier orbital energies were calculated from the onset values of the first oxidation and reduction waves setting the ferrocene HOMO energy to –5.1 eV versus vacuum (Table 3). As a result of the increase in HOMO energies with growing number of thiophene units, the electrochemical gaps decreased from 2.37 eV for DCC1T to 1.96 eV for DCC4T. In

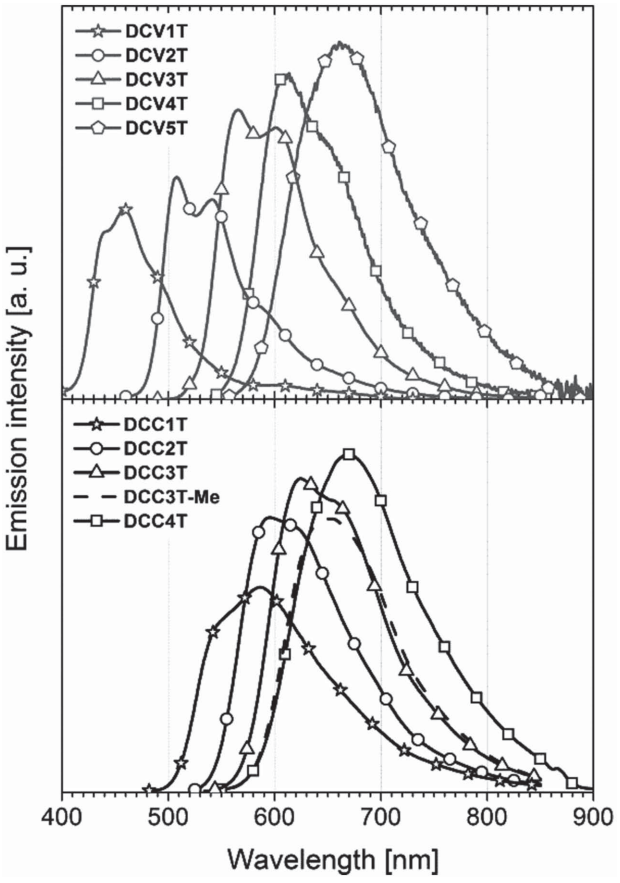

Figure 7. Emission spectra of DCC*n*T (bottom) and DCV*n*T oligomers (top) measured in dichloromethane at room temperature.

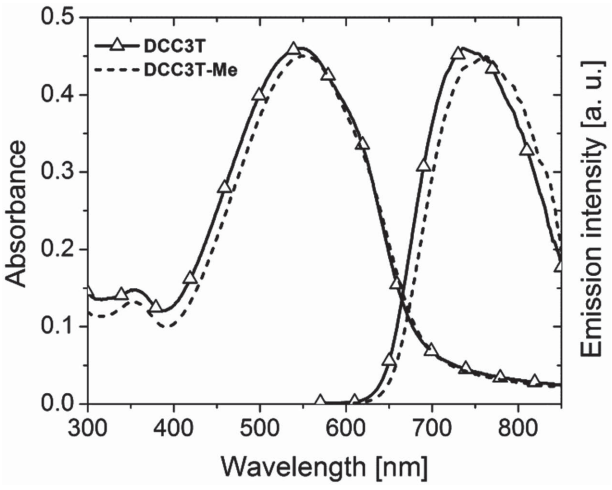

Figure 8. Absorbance and emission spectra of DCC3T and DCC3T-Me in 30 nm thick films fabricated by vacuum-deposition onto quartz substrates.

Figure 9b, frontier orbital energies of DCC*n*Ts and DCV*n*Ts are plotted versus the number of double bonds in the oligomers. Comparing both oligomer series, derivatives with equal numbers of double bonds showed very similar HOMO/LUMO energies confirming the trend seen already for the maximum absorption wavelengths λ_{max}^{abs}. Regarding the potential of the oligomers as donor materials in organic solar cells, the LUMO energy levels of DCC3T (–3.71 eV), DCC3T-Me (–3.64 eV), and DCC4T (–3.68 eV) should be sufficiently high to provide a driving force for efficient electron transfer to the LUMO of the acceptor C_{60} (≈–4.1 eV).

Density functional theory (DFT) calculations [m062x (6–31g+(d))] have been performed on both series of A–D–A oligothiophenes. **Figure 10** displays the electronic distribution of the frontier orbitals of DCC-3T and DCV4T as examples, which comprise the same number of double bonds. The HOMO of both derivatives shows a delocalization of the electron density over the donor part up to the vinylic carbon adjacent to the terminal dicyanomethylene groups (labeled by arrows). The delocalization of the LUMO expands over the entire DCC3T and DCV4T π-conjugated path. The LUMO+1 showed a pronounced shift of the electronic density to the acceptor parts on both derivatives. This virtual energetically high lying orbital

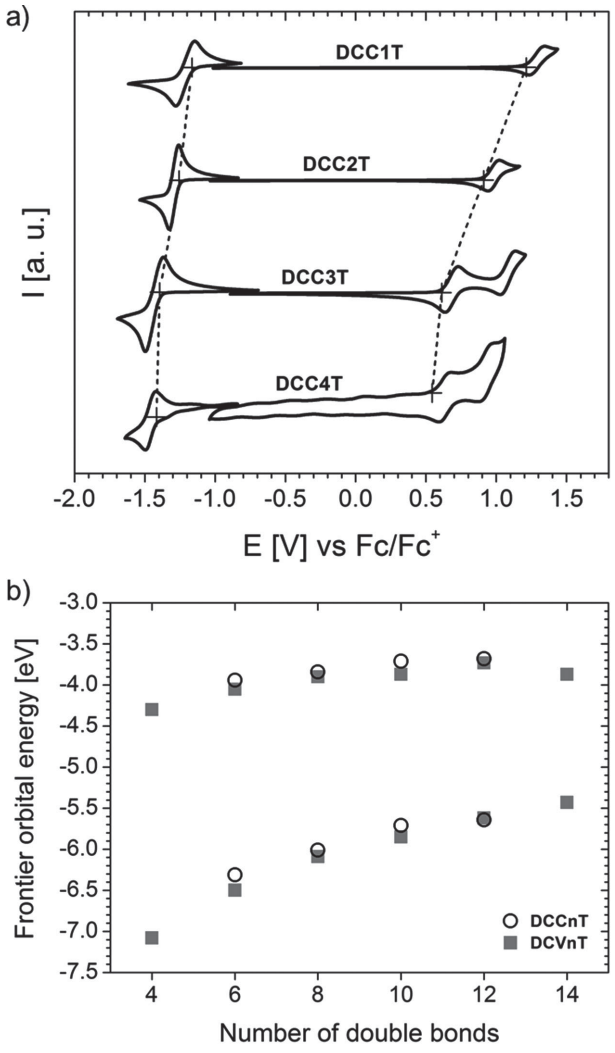

Figure 9. a) Cyclic voltammograms of the DCC*n*T oligomer series measured in dichloromethane and $TBAPF_6$ (0.1 M) as electrolyte, scan rates were 100 mV s^{-1} and potentials are given versus Fc/Fc^+. b) Frontier orbital energies of DCC*n*Ts and DCV*n*Ts derived from electrochemical data versus the number of double bonds in the oligomers.

can be stabilized experimentally by the presence of solvent and therefore can be responsible for the charge transfer character of the electronic transition.

The analysis of the calculated molecular orbital energies (Table S5, Supporting Information) supports as well the trends found in the electrochemical studies. In **Figure 11** the experimentally determined frontier orbital energies are displayed elucidating the effect of the extrinsic double bonds in DCC3T: Compared to the DCV-derivatives DCV3T and DCV4T, the HOMO and the LUMO are lifted up in energy. However, for the derivatives with equal numbers of double bonds (DCC3T vs DCV4T), the band gap comes out nearly equal (2.0 eV and 1.98 eV), and both are as expected significantly smaller than this of DCV3T (2.19 eV), which corresponds to the findings in optical spectroscopy.

The destabilization of the HOMO and LUMO energies in DCC3T denotes an improved donor and reduced acceptor strength related to the DCV-derivatives. By keeping the acceptor groups unaffected, the lengthening of the π-conjugated system by two double bonds (DCV3T ð DCC3T) causes a significant raising of the HOMO energy level by 0.38 eV compared to the effect of the lengthening by one thiophene unit (DCV3T ð DCV4T), which amounts to 0.24 eV. We can explain this difference (0.14 eV) by the more effective aromatic stabilization in a thiophene ring with regard to two exocyclic double bonds. In contrast to the nearly unaffected LUMO energy levels in the DCV-series, the LUMO of DCC3T is raised by 0.16–0.19 eV, which can be ascribed as well to the loss of aromatization energy.

2.5. Photovoltaic Properties

To evaluate the photovoltaic properties of DCC3T and DCC3T-Me as donor in combination with C_{60} as acceptor, planar heterojunction (PHJ) organic solar cells have been fabricated by thermal vacuum deposition. For both devices, the following layer sequence was employed: 15 nm C_{60} evaporated on ITO-coated glass, 6 nm donor material, 10 nm of undoped 9,9-bis{4-[di-(p-biphenyl)aminophenyl]}fluorene (BPAPF), followed by 45 nm BPAPF p-doped with NDP9 as hole transport layer (HTL), 1 nm NDP9, and 100 nm aluminum as top electrode. **Figure 12** displays the *J–V* characteristics (Figure 12a) and the external quantum efficiency (EQE) spectra (Figure 12b) in comparison to the absorbance spectra of the donors in vacuum-deposited neat films (Figure 12c). The corresponding device parameters are summarized in **Table 4**. PHJ cells of both, DCC3T and DCC3T-Me, showed excellent open circuit voltages (V_{OC}) of 1.00 V for DCC3T and an increased value of 1.05 V for DCC3T-Me which can be attributed to the low lying HOMO energies of the donor oligomers. Similar short circuit current densities (J_{SC}) of 5.3 and 5.0 mA cm^{-2} were determined for the DCC3T and DCC3T-Me devices, respectively. This is in accordance with very similar EQE spectra measured for both materials, which correlate well with thin film absorption profiles. The DCC3T-Me device showed an improved saturation in current density of 1.08, defined as $J(-1V)/J_{SC}$, and a considerably increased fill factor (FF) of 65% compared to values of 1.11 and 56%, respectively, for DCC3T devices. In total, the DCC3T-Me PHJ device yielded PCE of 3.4% outperforming the DCC3T cell with a PCE of 3.0%. We have as well seen this trend for methylated A–D–A quinquethiophenes, which gave an improved performance compared to all other substituted derivatives coming from special intermolecular interactions and thus optimal packing of the oligomers in the solid state.[15a] If we compare these results with PHJ solar cells made from DCV4T, which comprises the same number of double bonds and conjugation length as the novel DCC3T-derivatives, the DCC-terthiophenes clearly surpass the quaterthiophene DCV4T in all photovoltaic parameters, which showed a PCE of only 1.2% under comparable conditions (Table 4). At that point it is noteworthy, that typically terthiophenes such as DCV3T and C_{60} did not lead to an efficient exciton separation into charge carrier pairs at the interface, because of the low HOMO offset between the two materials which leads to poor solar cell performance.[12a]

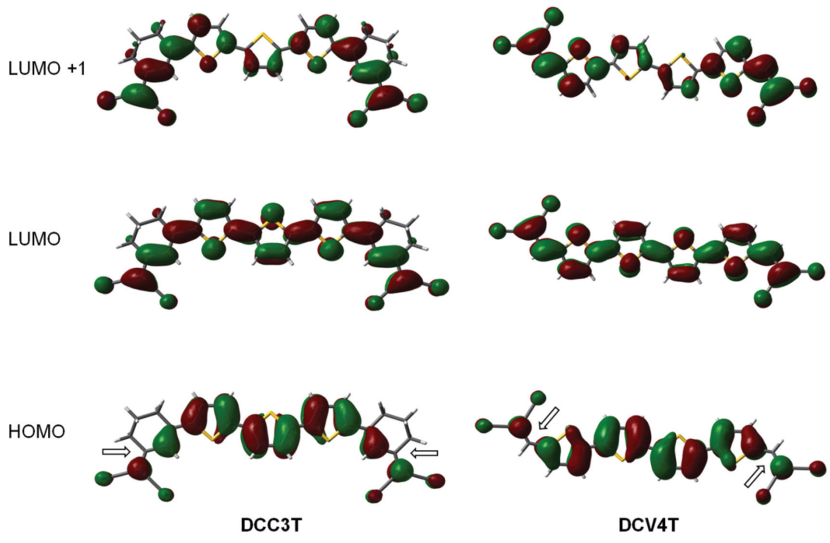

Figure 10. Representative electron density distribution of the frontier orbitals of DCC3T and DCV4T obtained by DFT-calculations (carbons in black, sulphurs in yellow, nitrogens in blue, and hydrogens in white).

DCC3T-Me as the best performing A–D–A oligomer in PHJs was additionally tested in BHJ solar cells. In the BHJ device stack, the neat donor layer employed in the PHJ setup was replaced by a 20 nm thick blend layer of donor and acceptor fabricated by co-evaporation of DCC3T-Me and C_{60} in a ratio of 2:1 by volume. During the deposition of the photoactive layer the substrate was heated to 90 °C. Despite the V_{OC} of the BHJ solar cells was slightly reduced to 0.99 V and the fill factor dropped to 53% compared to the PHJ device, a strongly enhanced J_{SC} of 8.5 mA cm^{-2} was found and led to a further improved PCE of 4.4% (Table 4).

This is as well represented in the EQE data of DCC3T-Me:C_{60}-BHJ devices achieving maximum values of 60% @ 500 nm compared to 35% in the PHJ devices, which can be assigned to the stronger thin film absorption (Figure 12c). Interestingly, this device performance of DCC-substituted terthiophene DCC3T-Me excels those of all 4T derivatives even

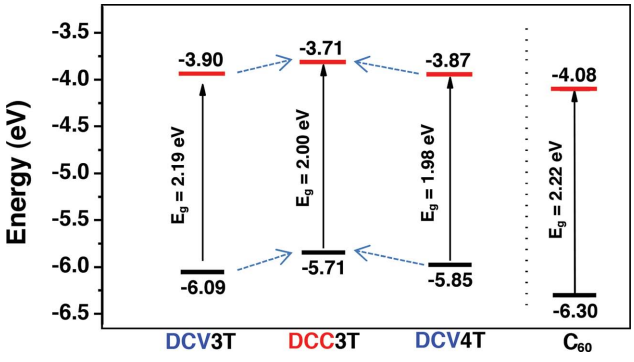

Figure 11. Representation of HOMO/LUMO energies of DCC3T in comparison to DCV3T and DCV4T and to C_{60} derived from electrochemical data. The HOMO/LUMO energy levels were determined from the onset of the oxidation and reduction waves (vide supra). The energy values of C_{60} are taken from the literature.[17]

the best one, which is methylated DCV4T-Me giving a PCE of 3.8% at a Voc of 0.98 V, a J_{sc} of 6.5 mA cm^{-2}, and a fill factor of 59%.[14]

3. Conclusion

In summary, a series of novel A–D–A oligothiophenes, from the mono- to the quarterthiophene, terminally substituted with the DCC acceptor has been synthesized. Structural, thermal, optoelectronic, and photovoltaic properties of the π-extended DCC*n*Ts were characterized and contrasted to the trends found for the series of dicyanovinyl (DCV)-substituted oligothiophenes DCV*n*T. We were able to bring out the influence of additional exocyclic, sterically fixed in *trans*-configuration, located between the acceptor and donor units in such A–D–A oligothiophenes. The direct comparison of the two series showed that (1) the DCC*n*Ts had increased melting temperatures and significantly enhanced solubilities including an odd–even effect as a function of the number of thiophene units due to molecular symmetry, whereas the thermal stability is somewhat smaller. (2) Great similarities in crystal packing were observed for DCC3T-Me and DCV5T-Me, which have the same substitution pattern and the same number of rings including efficient π–π-stacking of the oligothiophene cores. Both acceptor units, DCC and DCV, govern the 2D-arrangement in the molecular plane by multiple nonclassical hydrogen bonding. (3) The comparison of the optical properties of DCC- and DCV-capped oligomers resulted in a close correspondence of the absorption profiles for derivatives with equal number of double bonds, i.e., DCC*n*Ts and DCV(n + 1)Ts. (4) Electrochemical and theoretical investigations showed that despite having the same energy gap, the HOMO/LUMO energy levels for the DCC-derivatives are raised and more destabilized due to the aromatization energy of a thiophene ring versus two exocyclic double bonds. This result indicates that implementation of DCC-acceptor units lead to improved donor and reduced acceptor strength in the oligomers. (5) The incorporation of the DCC-terthiophenes DCC3T and DCC3T-Me as donor materials in vacuum-processed planar and bulk heterojunction solar cells resulted in a good photovoltaic performance (PCE ≤ 4.4%), which clearly outperformed all comparable DCV4T derivatives.

4. Experimental Section

Instruments and Measurements: NMR spectra were recorded on an Avance 400 spectrometer (^{1}H NMR: 400 MHz, ^{13}C NMR: 100 MHz) or a Bruker AMX 500 (^{1}H NMR: 500 MHz, ^{13}C NMR: 125 MHz), at 25 °C or 100 °C, respectively. Chemical shift values (δ) are expressed in parts per million using residual solvent protons (^{1}H NMR, δ_H = 7.26 for $CDCl_3$, δ_H = 2.50 for DMSO-d_6, and δ_H = 5.93 for tetrachloroethane-d_2; ^{13}C NMR, δ_C = 77.0 for $CDCl_3$, δ_C = 39.43 for DMSO-d_6, and δ_C = 74.20 tetrachloroethane-d_2) as internal standard. The splitting patterns are designated as follows: s (singlet), d (doublet), and m (multiplet). The

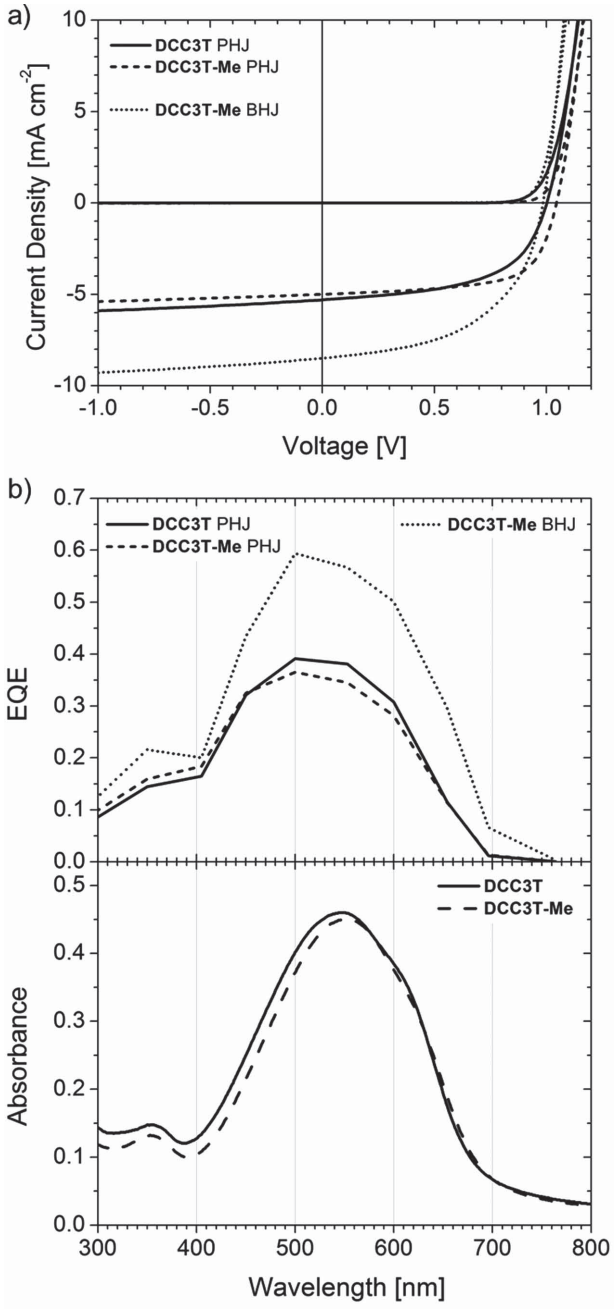

Figure 12. a) *J–V* characteristics of PHJ and BHJ solar cells containing novel DCC derivatives DCC3T and DCC3T-Me as donor material; b) corresponding external quantum efficiency spectra c) compared to absorbance spectra of thin films (30 nm) fabricated by vacuum-deposition onto quartz substrates.

assignments are Th*H* (thiophene protons), Me*H* (methyl protons), and V*H* (vinyl protons). GC-MS (EI) mass spectra were recorded on a Varian Saturn 2000, CI mass spectra on a Finnigan MAT SSQ-7000, and MALDI-TOF mass spectra on a Bruker Daltonic Reflex III. Differential scanning calorimetric measurements (DSC) were performed on a Mettler Toledo DSC823^e under argon atmosphere at a heating rate of 10 °C min^{-1}. Melting points were determined using a Büchi B-545 apparatus and were not corrected. Elemental analyses were performed on an Elementar Vario EL. Preparative column chromatography was performed on glass columns packed with silica gel (Merck Silica 60, particle size 40--43 μm). Optical solution measurements were carried out in 1 cm cuvettes with Merck Uvasol grade solvents; absorption spectra were recorded on a Perkin Elmer Lambda 19 spectrometer and corrected fluorescence spectra were recorded on a Perkin ElmerLS 55 fluorescence spectrometer. Thin film absorption spectra were recorded on a Shimadzu UV-2101/3101 UV–vis spectrometer. The thin film emission spectra were recorded with an Edinburgh Instruments FSP920 fluorescence spectrometer. Cyclic voltammetry experiments were performed with a computer-controlled Metrohm Autolab PGSTAT30 potentiostat in a three-electrode single-compartment cell with a platinum working electrode, a platinum wire counter electrode, and an Ag/AgCl reference electrode. All potentials were internally referenced to the ferrocene/ferrocenium couple. X-ray diffraction data of DCC3T-Me were collected on a Agilent SuperNova, Cu at zero, Atlas CCD using graphite-monochromated Cu Kα radiation. Data collection strategy was performed with the APEX2 software, data reduction, and cell refinement with SAINT. DCC3T-Me: $C_{32}H_{24}N_4S_3$, $M_r = 560.73$, dark-green platelet, $0.39 \times 0.10 \times 0.06$ mm^3, monoclinic, C2/c, $a = 21.3166(12)$ Å, $b = 15.0156(7)$ Å, $c = 9.1933(5)$ Å, $\beta = 118.089(8)°$, $V = 2596.0(3)$ Å^3, $Z = 4$, $\mu = 2.850$ mm^{-1}, $d_x = 1.435$ g cm^{-3}, $T = 150$ K. 4754 reflections collected ($\theta_{max} = 73.723°$) and merged to 2541 independent data ($R_{int} = 0.023$); final R indices ($I > 2\sigma(I)$): $R1 = 0.0402$, $wR2 = 0.0457$. Detailed crystallographic data for structure DCC3T-Me has been deposited with the Cambridge Crystallographic Data Centre as supplementary publication CCDC 1025975. Details on measurement and refinement are given in the Supporting Information.

Quantum Chemical Calculations: Density functional theory was employed with the hybrid functionals B3LYP and the basis set 6–31G* from the NWChem package.[18]

Thin Film and Device Fabrication: Thin films and planar heterojunction solar cell devices were prepared by thermal vapor deposition in ultra-high vacuum at a base pressure of 10^{-7} mbar onto the substrate at room temperature. Thin films for absorption and emission measurements were prepared on quartz substrates; solar cells on tin-doped indium oxide (ITO) coated glass (Thin Film Devices, USA, sheet resistance of 30 Ω sq^{-1}). Layer thicknesses were determined during evaporation by using quartz crystal monitors calibrated for the respective material. The thin films prepared for absorption and emission measurements are approximately 30 nm thick. The bulk-heterojunction solar cell was prepared layer by layer without breaking the vacuum using the following layer structure: ITO; 15 nm C_{60}; 20 nm blend layer of DCC3T-Me and C_{60} (ratio 2:1 by volume) prepared by co-evaporation on the heated substrate (90 °C), 10 nm 9,9-bis{4-[di-(p-biphenyl)aminophenyl]} fluorene (BPAPF), 50 nm BPAPF p-doped with NDP9 (purchased from Novaled AG Germany, 10 wt%), 1 nm NDP9, 100 nm aluminum.

Photovoltaic Characterization: *J–V* and EQE measurements were carried out in a glove box with nitrogen atmosphere. *J–V* characteristics were measured using a source-measure unit (Keithley SMU 2400) and an AM 1.5G sun simulator (KHS Technical Lighting SC1200). The intensity was monitored with a silicon photodiode (Hamamatsu S1337), which was calibrated at Fraunhofer ISE, Freiburg, Germany. The mismatch between the spectrum of the sun simulator and the solar AM 1.5G spectrum was taken into account for the calculation of current density. For well-defined active solar cell areas, aperture masks (2.76 mm^2) were used. Simple EQE measurements were carried out using the sun simulator in combination with color filters for monochromatic illumination. The illumination intensities were measured with a silicon reference diode (Hamamatsu S1337).

Reagents and Chemicals: 2,5-Bis(trimethylstannyl)thiophene 1,[19] 5,5′-bis(trimethylstannyl)-2,2′-bithiophene 2,[20,21] 3-bromocyclohex-2-enone 3,[22–24] 3-methoxy-2-cyclohex-2-enon 7,[25] and 2,5-bis(trimethylstannyl)-3,4-dimethylthiophen 10[26] were prepared according to published literature procedures. 2,5-Dibromothiophene 6 was purchased from Aldrich. Malonitrile and β-alanine were purchased from Merck. *n*-Butyl lithium (1.6 M solution in hexanes) was purchased from Acros. All synthetic steps were carried out under argon atmosphere.

3,3′-(Thien-2,5-diyl)bis(cyclohex-2-enone) 4: A mixture of 2,5-bis-(trimethylstannyl)thiophene 1 (200 mg, 488 μmol), 3-bromocyclohex-2-enone 3 (179 mg, 1.03 mmol), and tetrakis(triphenylphosphine)

Table 4. Photovoltaic characteristics of planar (PHJ) solar cell devices containing DCC3T and DCC3T-Me as donor component and C_{60} as acceptor in comparison to DCV4T and of bulk heterojunction (BHJ) cells with DCC3T-Me.

Donor oligomer	Device type	V_{OC} [V]	J_{SC} [mA cm^{-2}]	FF [%]	PCE [%]	Saturation[a)]	Intensity [mW cm^{-2}]
DCC3T	PHJ	1.00	5.3	56	3.0	1.11	93
DCC3T-Me	PHJ	1.05	5.0	65	3.4	1.08	92
DCV4T[b)]	PHJ	0.97	2.9	42	1.2	1.30	100
DCC3T-Me	BHJ	0.99	8.5	53	4.4	1.09	87

[a)]Saturation defined as $J(-1\ V)/J_{SC}$, i.e., voltage bias dependence of the current in reverse direction; [b)]Data taken from the literature.[12c]

palladium(0) (28 mg, 24 µmol) in degassed DMF (3 mL) was stirred at 80 °C for 3 h. Upon cooling to –20 °C, the resulting precipitate was filtered off and washed thoroughly with water. The filtrate was poured into dichloromethane (50 mL), washed with water (3 × 50 mL), dried over $MgSO_4$, filtered, and concentrated under reduced pressure. Recrystallization of the combined solids from *n*-hexane/dichloromethane provided compound 4 (117 mg, 430 µmol, 88% yield) as yellow needles. Mp 149 °C (DSC);^{1}H NMR (DMSO-d_6, δ ppm) 7.69 (s, 2H, Th*H*), 6.34 (s, 2H, V*H*), 2.78 (t, 4H, J = 5.7 Hz), 2.38 (t, 4H, J = 6.6 Hz), 2.06–2.00 (m, 4H). ^{13}C NMR (DMSO-d_6, δ ppm) 198.12, 151.56, 144.28, 129.56, 122.70, 36.75, 27.02, 21.87. MS (EI) m/z: 272 [M$^+$]; Elemental analysis for $C_{16}H_{16}O_2S$: calculated. C, 70.56; H, 5.92; S, 11.77%; found: C, 70.41; H, 5.75; S, 11.58%.

3,3′-[(2,2′-Bithien)-5,5′-diyl]bis(cyclohex-2-enone) 5: A mixture of 5,5′-bis(trimethylstannyl)-2,2′-bithiophene **2** (200 mg, 406 µmol), 3-bromocyclohex-2-enone 3 (156 mg, 894 µmol), and tetrakis-(triphenylphosphine)palladium(0) (24 mg, 20 µmol) in degassed DMF (5 mL) was stirred at 80 °C for 3 h. Upon cooling to –20 °C, the resulting precipitate was filtered off and thoroughly washed with methanol. The filtrate was poured into dichloromethane (50 mL), washed with water (3 × 50 mL), dried over $MgSO_4$, filtered, and concentrated under reduced pressure. Recrystallization of the combined solids from *n*-hexane/dichloromethane provided diketone **5** (127 mg, 358 µmol, 88% yield) as orange needles. Mp 214 °C (DSC);^{1}H NMR (DMSO-d_6, 100 °C, δ ppm) 7.57 (d, 2H, J = 4.0 Hz, Th*H*), 7.44 (d, 2H, J = 4.0 Hz, Th*H*), 6.27 (s, 2H, V*H*), 2.79 (t, 4H, J = 5.5 Hz), 2.39 (t, 4H, J = 6.6 Hz), 2.10–2.05 (m, 4H). ^{13}C NMR (DMSO-d_6, 100 °C, δ ppm) 196.91, 150.88, 141,34, 137,87, 128,77, 125.71, 121,66, 36.27, 26.80, 21.43. MS (CI) m/z: 355 [M+H$^+$]; Elemental analysis for $C_{20}H_{18}O_2S_2$: calculated. C, 67.77; H, 5.12; S, 18.09%; found: C, 67.73; H, 5.28; S, 18.25%.

3-(5-Bromothien-2-yl)cyclohex-2-enone 8: To a solution of 2,5-dibromothiophene 6 (10.07 g, 25.0 mmol) in diethyl ether (75 mL), stirred at –78 °C, *n*-butyl lithium (1.6 M solution in hexanes, 15.6 mL, 25.0 mmol) was added dropwise over 15 min. After stirring at –78 °C for 10 min, a solution of 3-methoxy-2-cyclohex-2-enon 7 (3.16 g, 25.0 mmol) in diethyl ether (30 mL) was added and stirring was continued for 15 min. The solution was warmed to 0 °C, stirred for 3 h, and subsequently allowed to warm to room temperature and stirred for 16 h. The reaction was quenched with brine (300 mL) and the product was extracted with diethyl ether (3 × 150 mL). The combined organic extracts were dried over $MgSO_4$, filtered, and the solvents were removed in vacuo. Column chromatography (silica gel, DCM) and subsequent recrystallization from *n*-hexane yielded ketone 8 (4.91 g, 19.1 mmol, 76% yield) as a colourless crystalline solid. Mp 90.5–92 °C;^{1}H NMR ($CDCl_3$, δ ppm) 7.12 (d, 1H, J = 4.0 Hz, Th*H*), 7.05 (d, 1H, J = 3.9 Hz, Th*H*), 6.29 (s, 1H, V*H*), 2.70 (t, 2H, J = 6.0 Hz), 2.45 (t, 2H, J = 6.6 Hz), 2.16–2.09 (m, 2H).^{13}C NMR ($CDCl_3$, δ ppm) 199.08, 151.19, 143.97, 131.20, 127.57, 122.80, 116.38, 37.18, 27.35, 22.29. MS (EI) m/z: 258 [M+H$^+$]; Elemental analysis for $C_{10}H_9BrOS$: calculated. C, 46.71; H, 3.53; S, 12.47%; found: C, 46.97; H, 3.59; S, 12.48%.

2-[3-(5-Bromothien-2-yl)cyclohex-2-en-1-ylidene]malonitrile 9: A solution consisting of 3-(5-bromothien-2-yl)cyclohex-2-enone 8 (4.00 g, 15.6 mmol), malonitrile (3.08 g, 46.7 mmol), and β-alanine (83 mg, 0.93 mmol) in a mixture of dichloroethane (100 mL) and ethanol (100 mL) was stirred under reflux for 6 days. The reaction mixture was allowed to cool to room temperature, the precipitate was filtered off and washed thoroughly with water. After concentration of the filtrate in vacuo to about half the volume and cooling to room temperature, the resulting precipitate was collected by filtration and washed with water to afford a second crop of 9 (overall: 4.40 g, 14.4 mmol, 93% yield) as an orange crystalline solid. Mp 195.5–197 °C;^{1}H NMR ($CDCl_3$, δ ppm) 7.23 (d, 1H, J = 3.9 Hz, Th*H*), 7.10 (d, 1H, J = 3.9 Hz, Th*H*), 7.01 (s, 1H, V*H*), 2.80 (t, 2H, J = 6.4 Hz), 2.74 (t, 1H, J = 5.9 Hz), 2.00 (p, 1H, J = 6.1 Hz).^{13}C NMR ($CDCl_3$, δ ppm) 168.85, 149.24, 143.88, 131.71, 128.64, 118.57, 118.25, 113.28, 112.46, 78.34, 29.06, 27.73, 21.11. MS (EI) m/z: 306 [M+H$^+$]; Elemental analysis for $C_{13}H_9BrN_2S$: calculated. C, 51.16; H, 2.97; N, 9.18; S, 10.51%; found: C, 51.38; H, 3.04; N, 9.15; S, 10.54%.

2,2′-[(Thien-2,5-diyl)bis(cyclohex-2-en-3-yl-1-ylidene)]dimalonitrile DCC1T: A solution consisting of 3,3′-(thien-2,5-diyl)bis(cyclohex-2-enone) 4 (390 mg, 1.43 mmol), malonitrile (570 mg, 8.59 mmol), and β-alanine (7 mg, 0.08 mmol) in a mixture of dichloroethane (5 mL) and ethanol (5 mL) was stirred under reflux for 7 days. The reaction mixture cooled to –18 °C, the precipitate was filtered off and recrystallized from dichloromethane to yield DCC1T (427 mg, 1.16 mmol, 81% yield) as an red crystalline solid. Mp 319 °C (DSC);^{1}H NMR (tetrachloroethane-d_2, 100 °C, δ ppm) 7.45 (s, 2H, Th*H*), 7.16 (s, 2H, V*H*), 2.80–2.74 (m, 8H), 1.01–1.96 (m, 4H).^{13}C NMR (tetrachloroethane-d_2, 100 °C, δ ppm) 168.29, 149.26, 146.40, 129.18, 120.56, 113.18, 112.48, 80.02, 29.34, 28.69, 21.51. MS (CI) m/z: 369 [M+H$^+$]; Elemental analysis for $C_{22}H_{16}N_4S$: calculated. C, 71.72; H, 4.38; N, 15.21; S, 8.70%; found: C, 71.98; H, 4.43; N, 15.26; S, 8.83%.

2,2′-[(2,2′-Bithien-5,5′-diyl)bis(cyclohex-2-en-3-yl-1-ylidene)] dimalononitrile DCC2T: A suspension consisting of 3,3′-(2,2′-bithien-5,5′-diyl)bis(cyclohex-2-enone) 5 (730 mg, 2.06 mmol), malonitrile (680 mg, 10.3 mmol), and β-alanine (10 mg, 0.11 mmol) in a mixture of dichloroethane (10 mL) and ethanol (10 mL) was stirred under reflux for 21 days. The reaction mixture was allowed to cool to room temperature, the precipitate was filtered off and recrystallized from dichloroethane to yield DCC2T (691 mg, 1.53 mmol, 74% yield) as a dark red solid. Mp 331 °C (DSC);^{1}H NMR (tetrachloroethane-d_2, 100 °C, δ ppm) 7.40 (d, 2H, J = 4.0 Hz, Th*H*), 7.10 (s, 2H, V*H*), 2.79–2.75 (m, 8H), 2.01–1.96 (m, 4H).^{13}C NMR was not possible due to low solubility. MS (CI) m/z: 451 [M+H$^+$]; Elemental analysis for $C_{26}H_{18}N_4S_2$: calculated. C, 69.31; H, 4.03; N, 12.43; S, 14.23%; found: C, 69.50; H, 3.96; N, 12.38; S, 14.22%.

2,2′-[(2,2′:5′,2″-Terthien-5,5″-diyl)bis(cyclohex-2-en-3-yl-1-ylidene)] dimalonitrile DCC-3T: A mixture of 2,5-bis(trimethylstannyl)thiophene 1 (767 mg, 1.87 mmol), 2-[3-(5-bromothien-2-yl)-cyclohex-2-en-1-ylidene] malonitrile 9 (1.20 g, 3.93 mmol), and tetrakis(triphenylphosphine) palladium(0) (108 mg, 94 µmol) in degassed DMF (30 mL) was stirred at 80 °C for 30 h. Upon cooling, the resulting precipitate was filtered off and washed several times with methanol and *n*-hexane. After drying, DCC3T (783 mg, 1.47 mmol, 79% yield) was obtained as a dark purple solid. Mp 290 °C;^{1}H NMR (tetrachloroethane-d_2, 100 °C, δ ppm) 7.36 (d, 2H, J = 4.0 Hz, Th*H*), 7.20 (s, 2H, Th*H*), 7.16 (d, 2H, J = 4.0 Hz, Th*H*), 6.99 (s, 2H, V*H*), 2.74–2.71 (m, 8H), 1.96–1.90 (m, 4H).^{13}C NMR (tetrachloroethane-d_2, 100 °C, δ ppm) 168.99, 150.23, 141.91, 141.66, 137.17, 130.06, 126.73, 125.75, 118.90, 113.76, 113.04, 77.88, 29.41,

28.33, 21.58. MALDI-TOF MS m/z: 532 [M$^+$]; Elemental analysis for $C_{30}H_{20}N_4S_3$: calculated. C, 67.64; H, 3.78; N, 10.52; S, 18.06%; found: C, 67.70; H, 3.79; N, 10.30; S, 17.89%.

2,2′-[(2,2′:5′,2″:5″,2‴-Quaterthien-5,5‴-diyl)bis(cyclohex-2-en-3-yl-1-ylidene)]dimalonitrile DCC4T: A mixture of 5,5′-bis(trimethylstannyl)-2,2′-bithiophene (1.00 mg, 2.03 mmol), 2-[3-(5-bromothien-2-yl) cyclohex-2-en-1-ylidene]malonitrile 9 (1.30 g, 4.27 mmol), and tetrakis(triphenylphosphine)palladium(0) (117 mg, 10 µmol) in degassed DMF (40 mL) was stirred at 80 °C for 16 h. Upon cooling, the resulting precipitate was filtered off and washed several times with methanol and *n*-hexane. The crude product was extracted in a *Soxhlet* extractor with chlorobenzene for 6 days. The extract was cooled to room temperature and the precipitate was filtered off to yield DCC4T (819 mg, 1.33 mmol, 66% yield) as a black solid. Mp 333 °C (DSC);^{1}H NMR (tetrachloroethane-d_2, 100 °C, δ ppm) 7.39 (d, 2H, J = 4.0 Hz, Th*H*), 7.21 (d, 2H, J = 3.9 Hz, Th*H*), 7.18 (d, 2H, J = 4.0 Hz, Th*H*), 7.15 (d, 2H, J = 3.9 Hz, Th*H*), 7.07 (s, 2H, V*H*), 2.78–2.75 (m, 8H), 2.00–1.95 (m, 4H).^{13}C NMR was not possible due to low solubility. MALDI-TOF MS m/z: 614 [M$^+$]; Elemental analysis for $C_{34}H_{22}N_4S_4$: calculated. C, 66.42; H, 3.61; N, 9.11; S, 20.86%; found: C, 66.59; H, 3.51; N, 8.92; S, 20.60%.

2,2′-{[3′,4′-Dimethyl-(2,2′:5′,2″-terthien-5,5″-diyl)]bis(cyclohex-2-en-3-yl-1-ylidene)}dimalonitrile DCC3T-Me: A mixture of 2,5-bis-(trimethylstannyl)-3,4-dimethylthiophene 10 (400 mg, 913 µmol), 2-[3-(5-bromothien-2-yl)cyclohex-2-en-1-ylidene]malonitrile 9 (586 mg, 1.92 mmol), and tetrakis(triphenylphosphine)palladium(0) (46 mg, 40 µmol) in degassed DMF (15 mL) was stirred at 80 °C for 16 h. Upon cooling, the resulting precipitate was filtered off and washed several times with methanol and *n*-hexane. After drying, DCC3T-Me (443 mg, 787 µmol, 86% yield) was obtained as a dark purple crystalline solid. Mp 305 °C (DSC);^{1}H NMR (tetrachloroethane-d_2, 100 °C, δ ppm) 7.42 (d, 2H, J = 4.0 Hz, Th*H*), 7.17 (d, 2H, J = 4.1 Hz, Th*H*), 7.02 (s, 2H, V*H*), 2.78–2.72 (m, 8H), 2.33 (s, 6H, Me*H*), 1.97–1.91 (m, 4H). ^{13}C NMR (tetrachloroethane-d_2, 100 °C, δ ppm) 169.75, 150.91, 141.96, 141.68, 137.91, 130.67, 130.16, 127.56, 118.38, 114.23, 113.47, 76.95, 29.51, 28.29, 21.56, 15.30. MALDI-TOF MS m/z: 560 [M$^+$]; Elemental analysis for $C_{32}H_{24}N_4S_3$: calculated. C, 68.54; H, 4.31; N, 9.99; S, 17.15%; found: C, 68.51; H, 4.18; N, 9.98; S, 16.99%.

Supporting Information

Supporting Information is available from the Wiley Online Library or from the author.

Acknowledgements

The authors would like to thank the German Research Foundation (DFG) for financial support in the framework of special program SPP 1355. The authors thank Novaled GmbH for providing NDP9.

Received: November 27, 2014
Revised: January 17, 2015
Published online: February 16, 2015

[1] Y. Chen, X. Wan, G. Long, *Acc. Chem. Res.* **2013**, *46*, 2645.
[2] J. E. Coughlin, Z. B. Henson, G. C. Welch, G. C. Bazan, *Acc. Chem. Res.* **2014**, *47*, 257.
[3] L. Dou, J. You, Z. Hong, Z. Xu, G. Li, R. A. Street, Y. Yang, *Adv. Mater.* **2013**, *25*, 6642.
[4] a) A. Mishra, P. Bäuerle, *Angew. Chem.* **2012**, *124*, 2060; b) A. Mishra, P. Bäuerle, *Angew. Chem. Int. Ed.* **2012**, *51*, 2020.
[5] M. C. Scharber, N. S. Sariciftci, *Prog. Polym. Sci.* **2013**, *38*, 1929.
[6] a) J. Zhou, Y. Zuo, X. Wan, G. Long, Q. Zhang, W. Ni, Y. Liu, Z. Li, G. He, C. Li, B. Kan, M. Li, Y. Chen, *J. Am. Chem. Soc.* **2013**, *135*, 8484; b) B. Kan, Q. Zhang, M. Li, W. Ni, G. Long, Y. Wang, X. Yang, H. Feng, Y. Chen, *J. Am. Chem. Soc.* **2014**, *136*, 15529.
[7] a) T. S. van der Poll, J. A. Love, T.-Q. Nguyen, G. C. Bazan, *Adv. Mater.* **2012**, *24*, 3646; b) A. K. K. Kyaw, D. H. Wang, V. Gupta, J. Zhang, S. Chand, G. C. Bazan, A. J. Heeger, *Adv. Mater.* **2013**, *25*, 2397; c) V. Gupta, A. K. K. Kyaw, D. H. Wang, S. Chand, G. C. Bazan, A. J. Heeger, *Sci. Rep.* **2013**, *3*, 1965.
[8] Y. Zou, J. Holst, Y. Zhang, R. J. Holmes, *J. Mater. Chem. A* **2014**, *2*, 12397.
[9] Y.-H. Chen, L.-Y. Lin, C.-W. Lu, Z.-Y. Huang, H.-W. Lin, F. Lin, P.-H. Wang, Y.-H. Liu, K.-T. Wong, J. Wen, D. J. Miller, S. B. Darling, *J. Am. Chem. Soc.* **2012**, *134*, 13616.
[10] K. Cnops, B. P. Rand, D. Cheyns, B. Verreet, M. A. Empl, P. Heremans, *Nat. Commun.* **2014**, *5*, 3406.
[11] K. Schulze, C. Uhrich, R. Schüppel, K. Leo, M. Pfeiffer, E. Brier, E. Reinold, P. Bäuerle, *Adv. Mater.* **2006**, *18*, 2872.
[12] a) C. Uhrich, R. Schüppel, A. Petrich, M. Pfeiffer, K. Leo, E. Brier, P. Kilickiran, P. Bäuerle, *Adv. Funct. Mater.* **2007**, *1*, 2991; b) R. Schüppel, K. Schmidt, C. Uhrich, K. Schulze, D. Wynands, J. L. Bredas, E. Brier, E. Reinold, H. B. Bu, P. Bäuerle, B. Männig, M. Pfeiffer, K. Leo, *Phys. Rev. B* **2008**, *77*, 085311; c) R. Fitzner, E. Reinold, A. Mishra, E. Mena-Osteritz, H. Ziehlke, C. Körner, K. Leo, M. Riede, M. Weil, O. Tsaryova, A. Weiß, C. Uhrich, M. Pfeiffer, P. Bäuerle, *Adv. Funct. Mater.* **2011**, *21*, 897.
[13] K. Schulze, M. Riede, E. Brier, E. Reinold, P. Bäuerle, K. Leo, *J. Appl. Phys.* **2008**, *104*, 074511.
[14] R. Fitzner, C. Elschner, M. Weil, C. Uhrich, C. Körner, M. Riede, K. Leo, M. Pfeiffer, E. Reinold, E. Mena-Osteritz, P. Bäuerle, *Adv. Mater.* **2012**, *24*, 675.
[15] a) R. Fitzner, E. Mena-Osteritz, A. Mishra, G. Schulz, E. Reinold, M. Weil, C. Körner, H. Ziehlke, C. Elschner, K. Leo, M. Riede, M. Pfeiffer, C. Uhrich, P. Bäuerle, *J. Am. Chem. Soc.* **2012**, *134*, 11064; b) R. Meerheim, C. Körner, K. Leo, *Appl. Phys. Lett.* **2014**, *105*, 063306.
[16] K. Staub, G. A. Levina, S. Barlow, T. C. Kowalczyk, H. Lackritz, M. Barzoukas, A. Fort, S. R. Marder, *J. Mater. Chem.* **2003**, *13*, 825.
[17] Q. Xie, F. Arias, L. Echegoyen, *J. Am. Chem. Soc.* **1993**, *115*, 9818.
[18] M. Valiev, E. J. Bylaska, N. Govind, K. Kowalski, T. P. Straatsma, H. J. J. Van Dam, D. Wang, J. Nieplocha, E. Apra, T. L. Windus, W. A. de Jong, *Comput. Phys. Commun.* **2010**, *181*, 1477.
[19] C. van Pham, R. S. Macomber, H. B. Mark, Jr , H. Zimmer, *J. Org. Chem.* **1984**, *49*, 5250.
[20] S. Kotani, K. Shiina, K. Sonogashira, *J. Organomet. Chem.* **1992**, *429*, 403.
[21] U. Asawapirom, R. Guentner, M. Forster, T. Farrell, U. Scherf, *Synthesis* **2002**, *9*, 1136.
[22] E. Piers, I. Nagakura, *Synth. Commun.* **1975**, *5*, 193.
[23] C. Shih, J. S. Swenton, *J. Org. Chem.* **1982**, *47*, 2825.
[24] M. E. Jimenez, K. Bush, J. Pawlik, L. Sower, J. W. Peterson, S. R. Gilbertson, *Org. Biomol. Chem.* **2007**, *5*, 3778.
[25] C.-F. Shu, Y.-C. Shu, Z.-H. Gong, *Chem. Mater.* **1998**, *10*, 3284.
[26] H. Ziehlke, R. Fitzner, C. Koerner, R. Gresser, E. Reinold, P. Bäuerle, K. Leo, M. K. Riede, *J. Phys. Chem. A* **2011**, *115*, 8437.